IEEE Access
Multidisciplinary | Rapid Review | Open Access Journal

Received January 13, 2022, accepted March 3, 2022, date of publication March 10, 2022, date of current version March 21, 2022.

Digital Object Identifier 10.1109/ACCESS.2022.3158365

Determination of Core Losses Using an Inverse Modeling Technique

OSARUYI OSEMWINYEN[1], AHMED HEMEIDA[1,2], FLORAN MARTIN[1], ISMET TUNA GÜRBÜZ[1], PAYAM SHAMS GHAHFAROKHI[3,4], AND ANOUAR BELAHCEN[1,4], (Senior Member, IEEE)

[1]Department of Electrical Engineering and Automation, Aalto University, FI-00076 Espoo, Finland
[2]Department of Electrical Engineering, Cairo University, Giza 12211, Egypt
[3]Department of Electrical Machines and Apparatus, Riga Technical University, LV-1658 Riga, Latvia
[4]Department of Electrical Power Engineering and Mechatronics, Tallinn University of Technology, 19086 Tallinn, Estonia

Corresponding author: Osaruyi Osemwinyen (osaruyi.osemwinyen@aalto.fi)

ABSTRACT This paper presents an inverse thermal modeling technique to determine the core losses from the temperature rise inside the transformer core. For this purpose, initially, a customized printed circuit board (PCB) with thermal sensors is used to measure the temperature rise. Afterward, a 3D magneto-thermal forward model is developed to validate the temperature rise. The accuracy of the forward model is checked by comparing the simulated core losses and temperature rise of the transformer with experimental measurements for different supply conditions. The results show that the forward model can accurately estimate the core losses with a maximum relative error of less than 2.7% and predict the temperature rise in the core with a maximum relative error of less than 6.2%. Lastly, after ensuring the accuracy of the forward model, an inverse modeling technique is applied to the 3D thermal model to predict the core losses of the transformer directly from the measured temperature rise. The accuracy of the inverse model in estimating the core losses is checked by comparing the results with experimental measurements. The novel approach for the PCB design besides the inverse model shows that the technique can be applied to estimate the core losses directly from the measured temperature rise inside the core with a relative error of 2.7% compared to experiments.

INDEX TERMS Core losses, inverse modeling, loss model, temperature measurement, thermal model, thermal sensors.

I. INTRODUCTION

The increasing use of electrical machines in transportation and rapid industrialization has created the need for designing more efficient electrical machines. The strategy used by designers in developing more efficient machines is to reduce the generated losses, which can be classified into core losses, resistive losses, and mechanical losses. Hence, accurate prediction and measurements of these losses are essential for the evaluation of efficiency, temperature distribution, and cooling requirements of the electrical machine. Core losses are one of the most important parameters considered during the designing stage of electrical machines. Therefore, accurate estimation and reduction of core losses are vital to designing efficient electrical machines [1].

Several analytical and numerical models were widely used by machine designers to estimate the core losses in magnetic materials [2]–[6]. Separation models were used in [2]–[4] to estimate the core losses. With this method, the total core losses were obtained as the summation of the hysteresis loss, eddy-current loss, and excess loss. An empirical model based on Steinmetz equation was presented in [6] and [5] to estimate the core losses. Although these models present a fast way to estimate the core losses; however, they are based on constant coefficients that require several measurements and fitting to identify. Moreover, the coefficients change with the flux density, frequency, and type of material [7].

Another approach used for estimating power losses is based on inverse thermal models. The main theory is that power losses generated in the different parts of an electrical machine contribute directly to heat. Therefore, by measuring the temperature rise at any point in a machine, the losses can be inversely determined. This principle was applied in [8]–[12] to estimate the power losses and thermal parameters of electrical machine. Calorimetric method described in [9] and [11] was used to determine the losses directly from

The associate editor coordinating the review of this manuscript and approving it for publication was Giambattista Gruosso.

the heat dissipation of the machine. Although a significant accuracy is reached with this method, the design and construction processes of the setup take a long time and can be unsuitable for industrial applications.

Using the lumped parameter thermal network (LPTN) in combination with the experimental measured temperature rise, the net power losses in an induction machine were segregated in [12] by inverse thermal method. This approach was used in [10], [13], and [14] to identify the thermal parameters used in the real-time prediction of stator and rotor temperature variations for condition motoring of electrical machines. Nevertheless, LPTN involves approximation of geometry and thermal material properties of the machine in nodes. Hence, the reliability and the accuracy of such thermal network is strongly affected by the model designer. Alternatively, in [8], highly accurate results were obtained by using a finite-element model (FEM) to validate the temperature rise that was measured with built-in resistance temperature detectors inside the machine. However, the built-in sensors in the machine parts are prone to failures, and also placing the sensors in the interior parts of the machine is difficult.

In this paper, we present a method to estimate the core losses in a transformer from the measured temperature rise inside the core by inverse modeling technique. We introduce a customized sensor board consisting of thermal sensors to access the interior part of the transformer and minimize the measurement noise. Initially, a 3D magneto-thermal model for the transformer is developed in COMSOL-Multiphysics to validate the measured temperature rise. After modeling the temperature rise properly with the forward model, the core losses are then predicted from the presented inverse thermal model with high accuracy.

The remainder of this paper is organized as follows. In Section 2, the measurement system is described in detail. The models developed based on the experimental measurements are presented in Section 3. Afterward, the applications of the models and obtained results are presented in Section 4. Then, in Section 5, the most important findings of this study are summarized.

II. EXPERIMENTAL MEASUREMENTS

Experimental measurements of core losses and temperature rise are performed at different cases of supply voltages under the sinusoidal excitation with the fundamental frequencies between 50-150 Hz on a single-phase shell-type transformer under no-load conditions. The transformer core is cut from electrical steel sheets with a lamination thickness of 0.5 mm, and the material grade is M400-50A. Figure 1(a) shows the transformer under test with the power supply feeding it. NI USB-6251 data acquisition device (DAQ_1) is used to retrieve the primary current i_1 and the induced voltage in the secondary side u_2 with respect to time. The core losses are computed from these measurements during the post-processing stage. The temperature rise of the transformer is measured with two thermal PCBs placed inside the transformer core, PT100 thermal sensors are embedded in the board as shown in Fig.1(b).

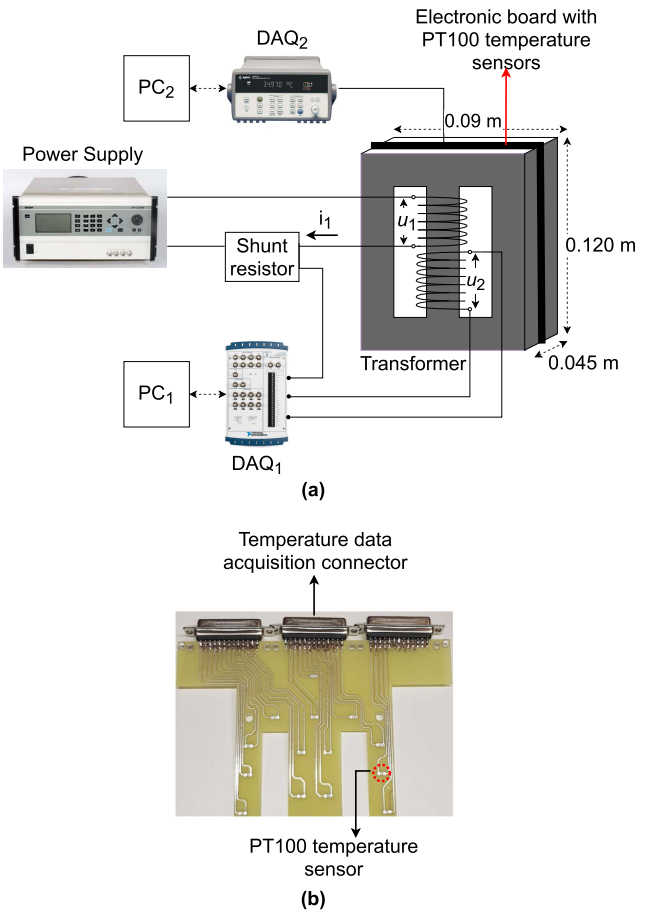

FIGURE 1. (a) Experimental measurement setup. (b) Electronic board with PT100 temperature sensors.

A. LOSS MEASUREMENT

The total loss consist of core and copper losses. Sinusoidal voltage u_1 is supplied to the primary winding of the transformer at no-load. The primary current i_1 is obtained through the shunt resistor connected in series to the input terminal and the induced voltage in the secondary side u_2 is measured directly from the secondary winding of the transformer. The magnetic flux density $B(t)$ in the middle limb section of the transformer is computed using (1).

$$B(t) = \frac{1}{N_2 A_{\text{lm}}} \int u_2(t) dt, \tag{1}$$

where N_2 is the number of turns in the secondary winding, and A_{lm} is the cross-sectional area of the middle limb. The magnetic field intensity $H(t)$ at the lamination surface is calculated from the measured no-load current using (2).

$$H(t) = \frac{N_1 i_1(t)}{l_{\text{av}}} \tag{2}$$

where N_1 is the number of turns in the primary winding and l_{av} is the mean length of flux path. The core loss density p_{tot} is obtained from the integral of (1) and (2) over one supply period T as given in (3).

$$p_{tot} = \frac{1}{T\rho}\int_0^T B(t)H(t)dt \tag{3}$$

where, ρ is the mass density of the core material. Using (4), the winding resistive losses P_R is computed taking into account the effect of temperature rise on the winding resistance. Here, only the DC component of the resistive losses P_R is considered.

$$P_R = I^2_{pri,rms}R_{dc,pri}(1 + \alpha\Delta T) \tag{4}$$

where, $R_{dc,pri}$ is the measured DC winding resistance, α is the thermal resistivity of copper, and ΔT is the change in temperature over the measurement duration.

B. THERMAL MEASUREMENT

The objective of the thermal measurement setup is to obtain temperature rise inside the transformer core and winding. For this purpose, two PCB boards with a thickness of 0.5 mm embedded with PT100 temperature sensors are used. The PCB is designed to perfectly match the geometry of the transformer core as shown in Fig. 1(b). Each board consists of 14 PT100 temperature sensors that are evenly placed over the geometry to accurately measure the temperature distribution of the transformer core during power switch ON. The sensors have a measurement range of −50℃ to 250℃ and can measure the temperature rise of the transformer with an accuracy of ±0.06℃. An Agilent 34970A data acquisition unit (DAQ_2) is connected to the sensor board serial output port. The transformer temperature rise is recorded for 4 hours under no-load conditions. The measured temperature is used to estimate the core losses by applying the inverse modeling technique. The results obtained are compared with the measured core density in Section IV-D to test the accuracy of the loss identification approach.

III. FORWARD MODELING

This section describes the electromagnetic loss model and thermal model used for simulating the temperature rise of the transformer that occurs in the real situation. The models are developed with COMSOL-Multiphysics. The major dimensions and the parameters used in the model design are shown in Table 1. The flow chart of the modeling technique is shown in Fig. 2. In the following parts of this section, each step will be explained in detail.

A. ELECTROMAGNETIC LOSS MODEL

A 2D electromagnetic model of the transformer is implemented to achieve an accurate quantification of the distribution of the core losses, taking into account the realistic flux density distribution. The model assumes that the flux distribution is constant in the core thickness direction. The 2D

TABLE 1. Transformer dimensions and parameters.

Quantity	Value
Rated Voltage, u_1	24V
Number of primary turns, N_1	60
Number of secondary turns, N_2	50
Lamination thickness	0.5 mm
Total number of laminations	90
Height×width of the transformer	120×90 mm
Mass density of core material, ρ	7650 kg/m^3
Thermal conductivity of core material, k	30 W/mK

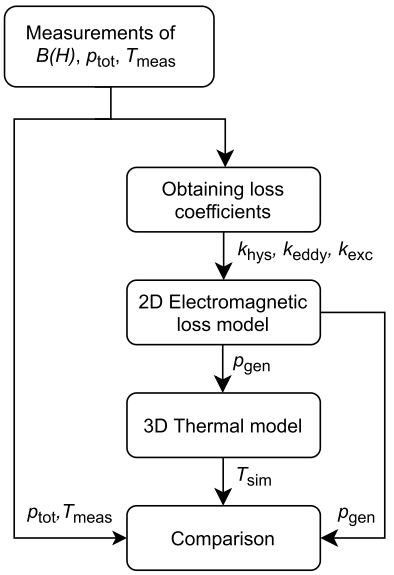

FIGURE 2. Forward modeling flow chart.

model description of the transformer used in the simulation with the mesh is shown in Fig. 3(a). To predict the flux density and loss distribution in the transformer core, time-stepping magnetic field simulation is carried out by applying sinusoidal voltage u_1 to the input terminal of the primary winding at no-load as shown in Fig. 3(b).

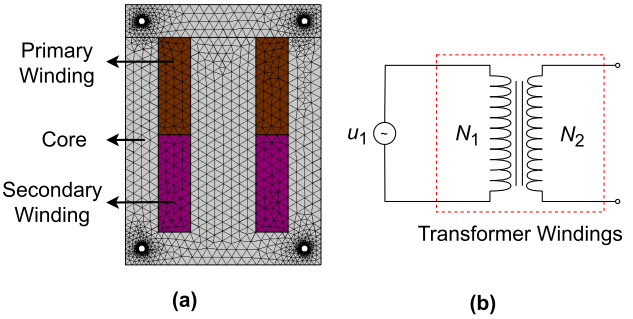

FIGURE 3. (a) 2D electromagnetic model with mesh. (b) Model supply circuit. Secondary side is open-circuited.

The core loss density $p_{fe,(sim)}$ is computed from the fundamental and harmonic component of the flux density

distribution by using (5) during FEM post-processing.

$$p_{\mathrm{fe,(sim)}} = K_{\mathrm{hys}} \sum_{i=1}^{N} f_{\mathrm{i}} \cdot B_{\mathrm{i}}^{n} + K_{\mathrm{eddy}} \sum_{i=1}^{N} f_{\mathrm{i}}^{2} \cdot B_{\mathrm{i}}^{2} + K_{\mathrm{exc}} \sum_{i=1}^{N} f_{\mathrm{i}}^{1.5} \cdot B_{\mathrm{i}}^{1.5} \quad (5)$$

where, N and f_{i} are the total number of harmonics and the frequency at each harmonic, $K_{\mathrm{hys}}, K_{\mathrm{eddy}}$, and K_{exc} are the hysteresis, eddy-current, and excess loss coefficients, respectively. These coefficients are obtained experimentally by fitting the coefficients of (5) to the measured core losses at different frequencies. Finally, the accuracy of the electromagnetic loss model is compared with the measured core losses. The comparisons are shown in the results section.

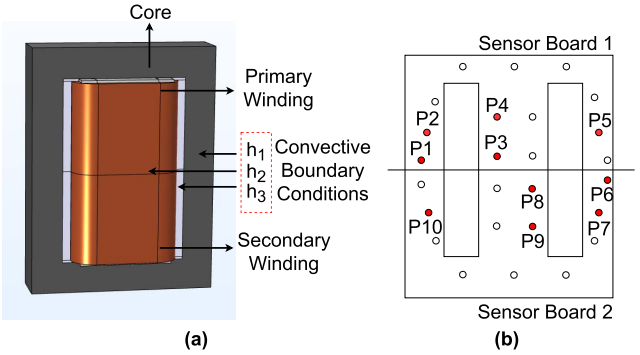

FIGURE 4. (a) 3D thermal model description. (b) Sensor location description in the core. Red marker indicates the sensors used in the measurements.

B. THERMAL MODEL

The 3D thermal model described in Fig. 4(a) is used to analyze the temperature rise distribution of the transformer. The locations of the sensors used for the measurements of temperature rise are given in Fig. 4(b). The physics used in the modeling is based on the first law of thermodynamics and Fourier's law. Mathematically, it can be expressed by the heat diffusion equation (6), which is the law governing heat transfer in electrical machines.

$$\rho C_{\mathrm{p}} \frac{\partial T}{\partial t} - \nabla(k \cdot \nabla T) = p_{\mathrm{gen}} \quad (6)$$

where C_p, k, T, and $p_{\mathrm{gen}} = p_{\mathrm{fe,(sim)}}$, are specific heat capacity, thermal conductivity, temperature, and heat source, respectively. The distribution of the core losses obtained in Section III-A and uniform loss density are coupled to the thermal model as the core heat source. The resistive loss obtained from (4) is used as the heat source in the primary winding region. To simplify the simulated geometry, homogenization approach used in [15] defined by (7) and (8) are applied to the specific heat capacity and mass density to account for the composite material properties. Due to the symmetricity of the transformer, only half of the geometry is used in the simulation.

$$C_{\mathrm{p}} = \lambda_1 C_{\mathrm{p},1} + (1 - \lambda_1) C_{\mathrm{p},2} \quad (7)$$

$$\rho = \lambda_1 \rho_1 + (1 - \lambda_1) \rho_2 \quad (8)$$

where, λ_1 is the filling factor of core/winding, $C_{\mathrm{p},1}$ is the constituent specific heat capacity of core/winding, $C_{\mathrm{p},2}$ is the constituent specific heat capacity of the insulation layer, ρ_1 is the mass density of core/winding, ρ_2 is the mass density of insulating material. The anisotropic property of the thermal conductivity of the core and winding are modeled in two directions by using (9) for the lapping direction and (10) for the transverse direction as in [15], which are expressed below:

$$k_{\mathrm{lp}} = \lambda_1 k_1 + (1 - \lambda_1) k_2 \quad (9)$$

$$k_{\mathrm{ts}} = k_2 \frac{(1 + \lambda_1)\, k_1 + (1 - \lambda_1)\, k_2}{(1 - \lambda_1)\, k_1 + (1 + \lambda_1)\, k_2} \quad (10)$$

Here, k_1 is the thermal conductivity of core/winding, and k_2 is the thermal conductivity of insulating material. Newton's law of cooling defined by (11) is assigned to the boundary surface as defined by (12)

$$h = \frac{q}{A \cdot (T - T_{\mathrm{ext}})} \quad (11)$$

$$h = \begin{cases} h_1, & \text{on the winding surface} \\ h_2, & \text{on the core surface} \\ h_3, & \text{on the surface between the core and winding} \end{cases} \quad (12)$$

where, q, T, T_{ext}, A, and h, are the surface heat flux, temperature, surrounding temperature, surface area, and heat transfer coefficient, respectively. However, determining the heat transfer coefficient h can be quite challenging, as it depends on various factors such as surface temperature, ambient properties, and the nature of surfaces. Furthermore, it is determined in [16] that during natural cooling, about 25-30% of the heat flux is evacuated from the surface through radiation. Hence it is important to consider the effect of radiation on the total heat transfer coefficient. In this paper, the heat transfer coefficients are determined analytically by using (13)

$$h = h_{\mathrm{conv}} + h_{\mathrm{rad}}. \quad (13)$$

Here h_{conv} and h_{rad} are natural convection and radiation coeffiients. The natural convection coefficient h_{conv} is calculated from the Nusselt number Nu similar to [17], which is given by (14) and the radiation coefficient is estimated by using (15) [18],

$$h_{\mathrm{conv}} = \frac{Nu \cdot k_{\mathrm{fld}}}{L_{\mathrm{c}}}, \quad (14)$$

$$h_{\mathrm{rad}} = \epsilon \cdot \sigma \cdot \left(T^2 - T_{\mathrm{ext}}^2\right) \cdot (T - T_{\mathrm{ext}}), \quad (15)$$

where k_{fld} is the fluid thermal conductivity, σ is the Stefan-Boltzmann constant, L_{c} is the characteristic length and ϵ emissivity of the cooling surfaces. The convective heat coefficient is calculated for each of the surfaces. The equivalent heat transfer coefficient h of the composite surface is estimated by using the area-based composite correlation given in (16),

$$h = \frac{h_1 A_1 + h_2 A_2 + \ldots}{A_{\mathrm{T}}}, \quad (16)$$

where A_T, h_1, h_2 ... and A_1, A_2 ... are the total surface area, heat transfer coefficients, and surface area of each surface considered, respectively. Figure 5 shows the plot of the convective coefficient of the transformer for different temperature gradients by considering the radiation effect on the boundary surfaces.

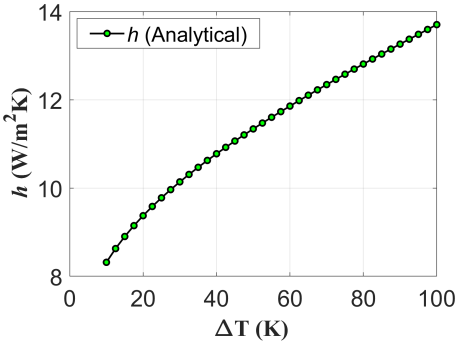

FIGURE 5. Transformer heat coefficient vs. different temperature gradient considering the radiation effect on natural convection.

IV. APPLICATIONS AND RESULTS

A. IDENTIFICATION OF LOSS COEFFICIENTS

Experimental measurements are carried out at sinusoidal excitation of different frequencies to estimate the loss coefficients. The flux density and core loss density are calculated from the measured no-load current i_1 and open-circuit voltage u_2 (see Fig. 1(a)) by using (1)-(3). The core loss coefficients are obtained by fitting Bertotti's formula (5) against the measured core loss density by using the flux density data at different excitation levels and frequencies in the range of 10 Hz - 150 Hz. Figure 6 shows the measured core losses and estimated core losses by using the fitted coefficients. The maximum relative fitting error of the coefficients is 5%.

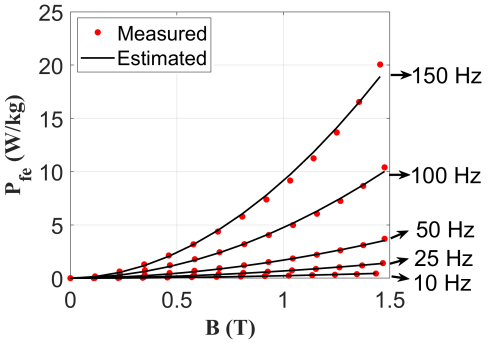

FIGURE 6. Comparison between measured core losses and estimated core losses with the following coefficients (5), $K_{hys} = 0.02$, $n = 1.82$, $K_{eddy} = 2.71 \times 10^{-4}$, $K_{exc} = 2.89 \times 10^{-7}$.

B. ELECTROMAGNETIC MODEL LOSS CALCULATION

Consequently, a time-varying magnetic field simulation is performed by applying a sinusoidal voltage to the primary winding of the magnetic model. Figure 7(a) shows the simulated flux density distribution of the 2D model. Fast Fourier Transform (FFT) is performed on the flux density distribution of each element to obtain the harmonic components of the flux density due to the non-linearity of the core material. The related core loss density distribution of the machine shown in Fig. 7(b) is calculated by using (5) from the identified loss coefficients. The simulated losses are compared with the measurements in Table 2 to validate the accuracy of the magnetic loss model.

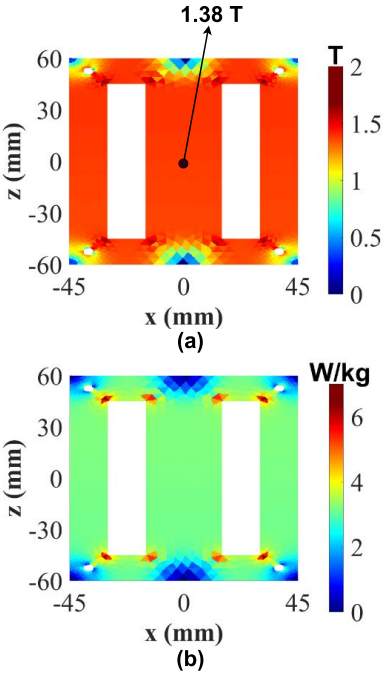

FIGURE 7. 2D electromagnetic loss model simulation ($u_1 = 24$V, $f = 50$ Hz). (a) Flux density distribution and (b) core loss density distribution.

TABLE 2. Comparison of the core losses at different frequencies.

f (Hz)	Core loss density (W/kg)		
	Measured	Simulated	Relative error (%)
10	0.38	0.39	2.63
25	1.20	1.21	0.83
50	3.04	3.05	0.33
100	8.66	8.64	0.23
150	16.78	16.77	0.06

The comparison shows that the magnetic model can accurately predict the losses at different frequencies. Hence, the results obtained can be used in the forward model to predict the temperature rise of the transformer.

C. THERMAL MODEL SIMULATIONS

Firstly, the core loss density distribution obtained from the 2D magnetic loss model and the winding loss obtained from (4) is inputted to the core and primary winding as a heat source of the thermal model as shown in Fig. 8(a). Next, the heat

source of the core region is replaced with uniform loss density obtained from the average core loss density of the magnetic loss model and the winding heat source remains constant as shown in Fig. 8(b). The model is simulated for 4 hours in both cases to obtain the temperature distribution shown in Fig. 9.

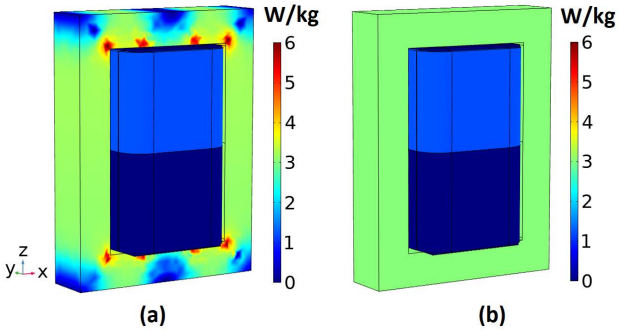

FIGURE 8. 3D electromagnetic heat source for $u_1 = 24$V, $f = 50$ Hz, for (a) distributed core loss density and for (b) uniform core loss density.

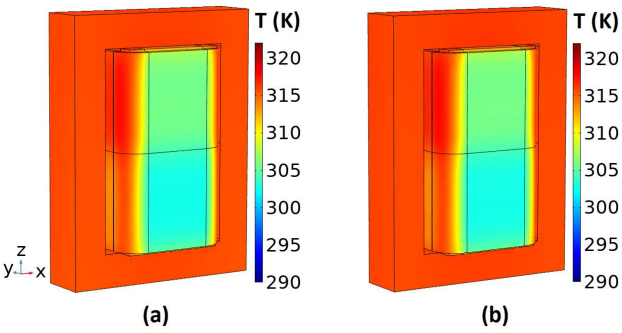

FIGURE 9. Temperature distribution for ($u_1 = 24$V, $f = 50$ Hz) after 4 hours with (a) distributed heat source and with (b) uniform heat source.

From Fig. 9, it can be observed that the temperature distribution is uniform in the transformer core region for the simulated cases. However, temperature variation is observed in the winding geometry. This is because the variation of losses inside the core and edges are insignificant with respect to the overall volume of the transformer core. Furthermore, the accuracy of the forward thermal model to simulate the transformer temperature rise distribution under different supply conditions is tested by comparing (Fig. 10) the simulated temperature rise with the measured temperature rise for each of the sensor locations inside the core and winding. To better represent the results obtained, three measurement sensor locations represented by points P1, P4, P5, and the winding temperature variation is compared in Fig. 10 for the distributed heat source simulation case. The steady-state temperature rise for all the measured sensor locations are compared with the simulated steady-state temperature rise of the transformer for the distributed loss source (DL) and uniform loss source (UL) in Table 3.

From the analysis of Fig. 10 and Table 3, it is observed that the thermal model can accurately simulate the temperature rise distribution with a relative error of less than 6.2% for all sensor locations in the core for the simulated cases.

TABLE 3. Forward model relative error comparison for different sensors located inside the core at steady-state condition. Core heat source: distributed loss (DL) and uniform loss (UL).

f (Hz)	Relative Error (%)									
	P1	P2	P3	P4	P5	P6	P7	P8	P9	P10
50 (DL)	1.84	2.42	3.71	2.52	5.34	1.92	2.63	3.02	1.33	4.38
50 (UL)	2.49	3.07	4.37	3.18	**6.14**	2.62	3.43	3.74	2.11	5.40
100 (DL)	1.37	1.45	1.87	2.86	1.61	1.74	2.94	1.73	3.33	0.79
100 (UL)	1.02	1.10	1.49	2.48	1.12	1.32	1.92	1.28	2.80	0.04
150 (DL)	0.23	0.15	0.77	0.31	0.67	0.03	0.47	1.10	0.63	2.22
150 (UL)	0.22	0.35	1.00	0.08	1.03	0.25	0.08	1.40	0.23	2.89

D. PREDICTION OF CORE LOSSES USING INVERSE MODEL TECHNIQUE

The main target of the inverse model is to estimate the core losses of the transformer at no-load from the measured temperature rise. The core heat source defined in (7) is assumed to be uniform and unknown. Since the temperature rise measured from different locations inside the core is a direct consequence of the core losses, the unknown core losses of the thermal model are predicted using the inverse method. The methodology used is presented in Fig. 11.

The flowchart shows that the inverse model takes as an input the measured and simulated core temperature rise for the different sensor locations at steady-state. The least-square non-linear approximation method is applied to minimize the error between the measured and simulated temperature rise iteratively over time until the best fit for the predicted core loss density $p_{\text{tot,(prd)}}$ is obtained. The routine is repeated for the different measurement cases and the results obtained are compared with the measured core loss density in Table 4.

TABLE 4. Core loss density comparison at different frequencies.

f (Hz)	Core loss density (W/kg)		
	Measured	Predicted	Relative error (%)
50	3.04	2.96	2.63
100	8.66	8.75	1.04
150	16.78	16.62	0.95

The results show that the inverse model accurately predicts the core loss density from the measured temperature inside the transformer core with a maximum difference of less than 2.7%. The results returned from the inverse model are unique for each measured case. In other words, each time the inverse model is run for the same case, a unique solution is obtained in terms of the core loss density. The predicted temperature rise for the obtained core loss density $p_{\text{tot,(prd)}}$ from the inverse model is compared against the measured temperature rise for different sensor locations P1, P4, P5, and the winding as shown in Fig. 12.

Figure 12 shows that the predicted temperature rise matches reasonably well against the measurement results.

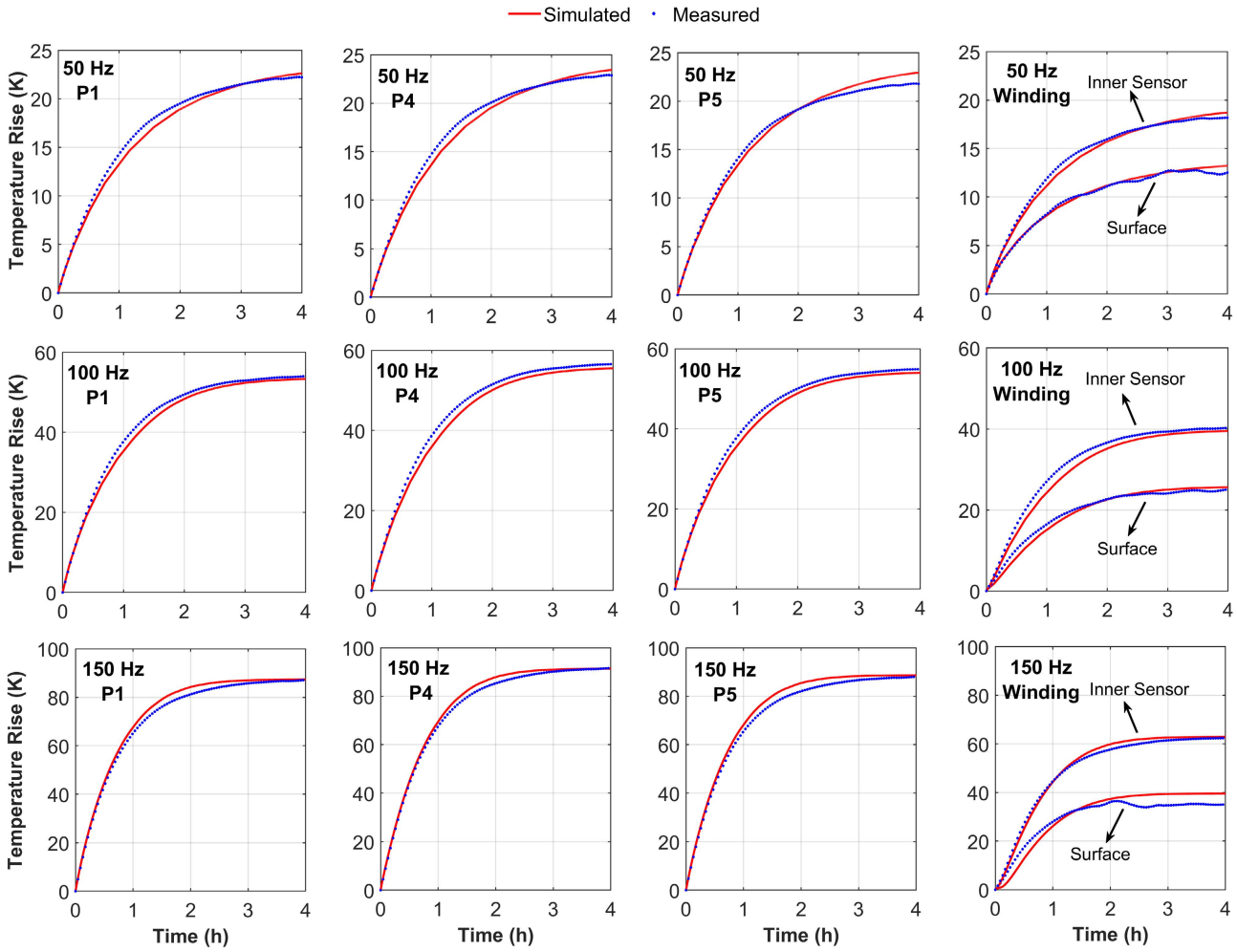

FIGURE 10. Comparison of the temperature rise from the simulations of forward model against the measurements.

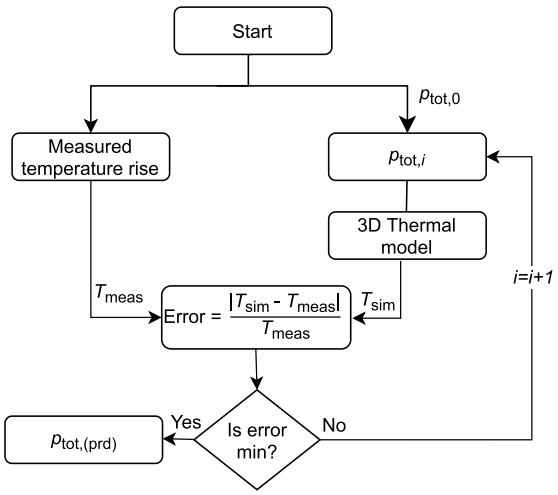

FIGURE 11. Inverse modeling flow chart.

A detailed comparison of the predicted temperature rise for each sensor located inside the core with the measured temperature rise is given in Table 5.

TABLE 5. The inverse model relative error comparison for different sensor locations inside the core at steady-state.

f (Hz)	Ralative Error (%)									
	P1	P2	P3	P4	P5	P6	P7	P8	P9	P10
50	0.05	0.52	1.79	0.64	**3.52**	0.08	0.86	1.17	0.42	2.78
100	0.08	0.16	0.55	1.55	0.18	0.39	0.99	0.33	1.86	0.92
150	0.22	0.29	0.34	0.73	0.38	0.39	0.72	0.74	0.84	2.23

The comparison in Table 5 shows that the inverse model accurately predicts the steady-state temperature rise distribution of the transformer with a relative error of less than 3.6% for all cases. However, when considering complex core geometry like the stator core of an induction machine, the basic assumption of a uniform heat source might increase the error in predicting the core losses because of the clear distinction of the yoke and teeth loss density. Therefore, defining a distributed heat source in the core and using the measured temperature rise for the different locations in the stator core will improve the accuracy of the inverse model results.

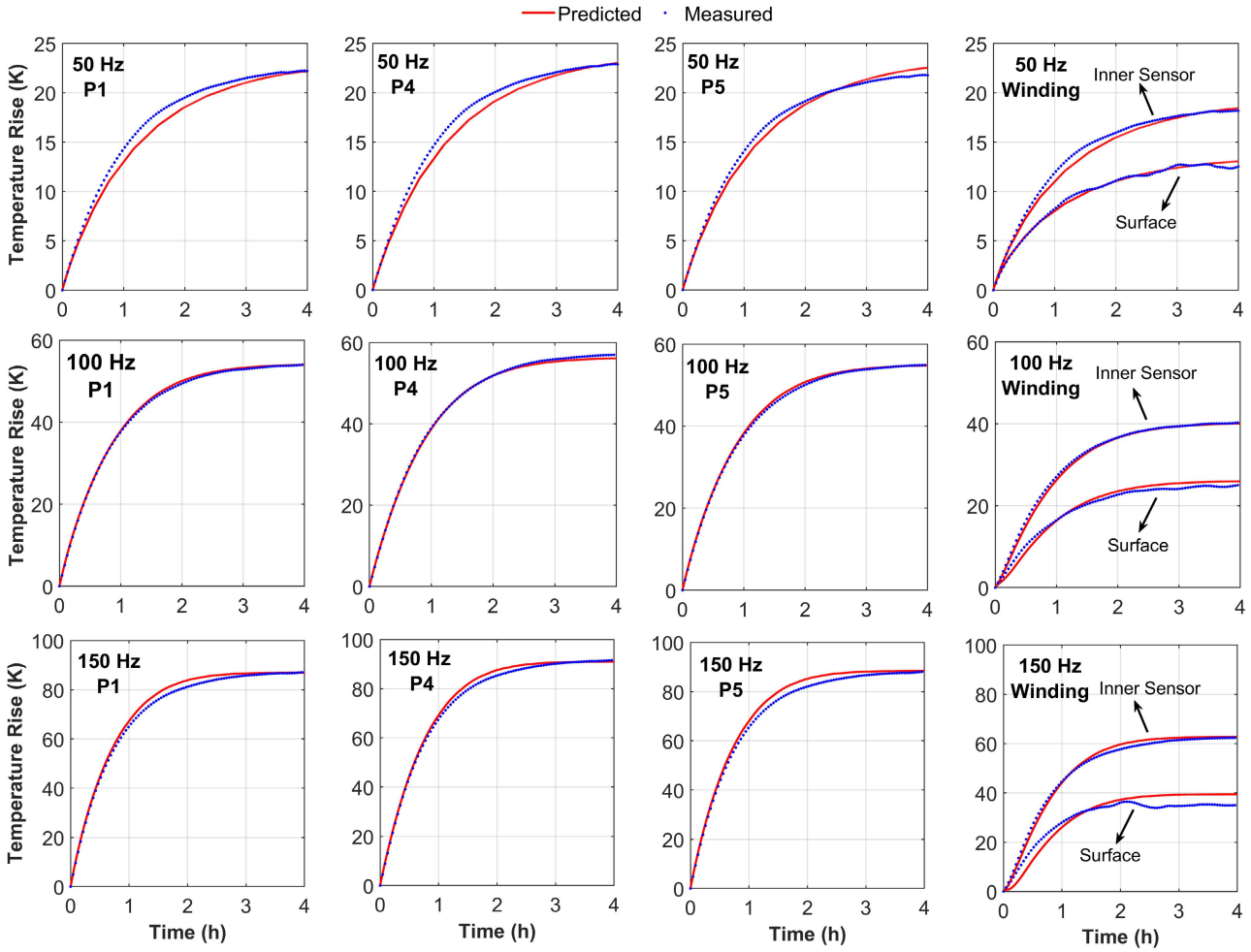

FIGURE 12. Comparison of the temperature rise from the predictions of inverse model against the measurements.

V. CONCLUSION

In this paper, we presented an inverse modeling technique to estimate the core losses of a transformer operating at no-load based on the measured temperature rise and its numerical thermal model. With the use of the customized sensor board, the method ensures the reliability of the temperature rise measurements, which is vital for the inverse modeling approaches. The proposed method can be applied on any electrical machine irrespective of the geometry with the appropriate design of the sensor board, which can be useful for condition monitoring and fault diagnosis purposes.

REFERENCES

[1] S. Kahourzade, N. Ertugrul, and L. Wen, "Loss analysis and efficiency improvement of an axial-flux PM amorphous magnetic material machine," *IEEE Trans. Ind. Electron.*, vol. 65, no. 7, pp. 5376–5383, Jul. 2018.

[2] K. Venkatachalam, C. R. Sullivan, T. Abdallah, and H. Tacca, "Accurate prediction of ferrite core loss with nonsinusoidal waveforms using only steinmetz parameters," in *Proc. IEEE Workshop Comput. Power Electron.*, Jun. 2002, pp. 36–41.

[3] G. Bertotti, "General properties of power losses in soft ferromagnetic materials," *IEEE Trans. Magn.*, vol. MAG-24, no. 1, pp. 621–630, Jan. 1988.

[4] A. Boglietti, A. Cavagnino, D. M. Ionel, M. Popescu, D. A. Staton, and S. Vaschetto, "A general model to predict the iron losses in PWM inverter-fed induction motors," *IEEE Trans. Ind. Appl.*, vol. 46, no. 5, pp. 1882–1890, Sep./Oct. 2010.

[5] H. Zhao, C. Ragusa, C. Appino, O. de la Barrière, Y. Wang, and F. Fiorillo, "Energy losses in soft magnetic materials under symmetric and asymmetric induction waveforms," *IEEE Trans. Power. Electron.*, vol. 34, no. 3, pp. 2655–2665, Mar. 2019.

[6] S. Barg, K. Ammous, H. Mejbri, and A. Ammous, "An improved empirical formulation for magnetic core losses estimation under nonsinusoidal induction," *IEEE Trans. Power Electron.*, vol. 32, no. 3, pp. 2146–2154, Mar. 2017.

[7] D. Kowal, P. Sergeant, L. Dupre, and L. Vandenbossche, "Comparison of iron loss models for electrical machines with different frequency domain and time domain methods for excess loss prediction," *IEEE Trans. Magn.*, vol. 51, no. 1, pp. 1–10, Jan. 2015.

[8] H. Vansompel, A. Yarantseva, P. Sergeant, and G. Crevecoeur, "An inverse thermal modeling approach for thermal parameter and loss identification in an axial flux permanent magnet machine," *IEEE Trans. Ind. Electron.*, vol. 66, no. 3, pp. 1727–1735, Mar. 2019.

[9] P. Rasilo, J. Ekstrom, A. Haavisto, A. Belahcen, and A. Arkkio, "Calorimetric system for measurement of synchronous machine losses," *IET Electr. Power Appl.*, vol. 6, no. 5, pp. 286–294, May 2012.

[10] J. Hey, A. C. Malloy, R. Martinez-Botas, and M. Lampérth, "Online monitoring of electromagnetic losses in an electric motor indirectly through temperature measurement," *IEEE Trans. Energy Convers.*, vol. 31, no. 4, pp. 1347–1355, Dec. 2016.

[11] L. Aarniovuori, J. Kolehmainen, A. Kosonen, M. Niemela, and J. Pyrhonen, "Calorimetric and input-output loss determination of SynRM," in *Proc. Int. Conf. Electr. Mach. (ICEM)*, Sep. 2014, pp. 79–85.
[12] D. G. Nair, A. Arkkio, and A. Haavisto, "Power loss segregation in electrical machines through calorimetry and inverse thermal modelling," *IET Electr. Power Appl.*, vol. 14, no. 7, pp. 1127–1133, Jul. 2020.
[13] P. N. Phuc, H. Vansompel, D. Bozalakov, K. Stockman, and G. Crevecoeur, "Inverse thermal identification of a thermally instrumented induction machine using a lumped-parameter thermal model," *Energies*, vol. 13, no. 1, p. 37, Dec. 2019.
[14] Zhu, Xiao, Lu, Wu, and Tao, "A simplified thermal model and online temperature estimation method of permanent magnet synchronous motors," *Appl. Sci.*, vol. 9, no. 15, p. 3158, Aug. 2019. [Online]. Available: https://www.mdpi.com/2076-3417/9/15/3158
[15] L. Idoughi, X. Mininger, F. Bouillault, L. Bernard, and E. Hoang, "Thermal model with winding homogenization and FIT discretization for stator slot," *IEEE Trans. Magn.*, vol. 47, no. 12, pp. 4822–4826, Dec. 2011.
[16] P. S. Ghahfarokhi, A. Kallaste, T. Vaimann, A. Rassolkin, and A. Belahcen, "Determination of natural convection heat transfer coefficient over the fin side of a coil system," *Int. J. Heat Mass Transf.*, vol. 126, pp. 677–682, Nov. 2018.
[17] D. A. Staton and A. Cavagnino, "Convection heat transfer and flow calculations suitable for electric machines thermal models," *IEEE Trans. Ind. Electron.*, vol. 55, no. 10, pp. 3509–3516, Oct. 2008.
[18] O. Meksi and A. O. Vargas, "Numerical and experimental determination of external heat transfer coefficient in small TENV electric machines," in *Proc. IEEE Energy Convers. Congr. Expo. (ECCE)*, Sep. 2015, pp. 2742–2749.

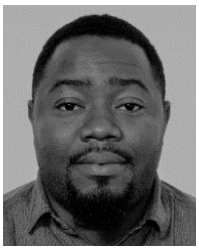

OSARUYI OSEMWINYEN received the B.Eng. degree in electrical and electronics engineering from the University of Benin, Nigeria, in 2010, and the M.Sc. (Tech.) degree from Aalto University, Finland, in 2017, where he is currently pursuing the Ph.D. degree with the Group of Electromechanics, as a Doctoral Researcher. His research interests include inverse thermal and magnetic modeling of electrical machines and energy conversion devices.

AHMED HEMEIDA received the B.Sc. and M.Sc. degrees from the Department of Electrical Power and Engineering, Cairo University, Egypt, in 2009 and 2012, respectively, and the Ph.D. degree from the Department of Electrical Energy, Metals, Mechanical Constructions and Systems, Ghent University, Belgium, in 2017. He worked as a Postdoctoral Research Assistant with the Department of Electrical Engineering, Aalto University, Finland, and as an Assistant Professor with the Department of Electrical Engineering, Cairo University. He is currently performing his research activities at Aalto University. His research interests include the modeling, control, and design of electrical machines.

FLORAN MARTIN received the Engineer Diploma degree of electrical engineering from Polytech Nantes and the M.S. degree in electrical engineering and the Ph.D. degree from the University of Nantes, in 2009 and 2013, respectively. He joined the Department of Electrical Engineering and Automation, Aalto University, in 2014, where he currently works as a Researcher with the Group of Computational Electromechanics. Since 2020, his staff scientist activities expand his horizon with the group of electric drive.

ISMET TUNA GÜRBÜZ received the B.Sc. (Tech.) degree in electrical and electronics engineering from Middle East Technical University, Turkey, in 2017, and the M.Sc. (Tech.) degree in electrical power and energy engineering from Aalto University, Finland, in 2019, where he is currently pursuing the D.Sc. (Tech.) degree in electrical engineering with the Group of Computational Electromechanics, as a Doctoral Researcher. His main research interests include the numerical modeling of magnetic materials and electrical machines.

PAYAM SHAMS GHAHFAROKHI received the B.Sc. degree in electrical power engineering from IAUN, Iran, in 2010, the M.Sc. degree in electrical power engineering from Newcastle University, U.K., in 2011, and the Ph.D. degree in electrical engineering and machines from the Tallinn University of Technology, Estonia, in 2019. He is currently a Senior Researcher and Postdoctoral Researcher with the Department of Electrical Machines and Apparatus, Riga Technical University, and the Department of Electrical Power Engineering and Mechatronics, Tallinn University of Technology. Moreover, he is a Visiting Researcher with the Electromechatronic Systems Research Centre (CISE), University of Beira Interior. His main research interest includes the electromagnetic design and thermal management of electrical machines for traction application purposes.

ANOUAR BELAHCEN (Senior Member, IEEE) was born in Morocco, in 1963. He received the M.Sc. (Tech.) and Doctor (Tech.) degrees from Aalto University (former Helsinki University of Technology), Finland, in 1998 and 2004, respectively. He is currently a Professor of energy and power at Aalto University, Finland, and a Professor of electrical machines with the Tallinn University of Technology, Estonia, where he has been acting as the Vice Dean of Education with the School of Electrical Engineering, since 2021. His research interests include numerical modelling of electrical machines, magnetic materials, coupled magneto-mechanical problems, magnetic forces, magnetostriction, and the fault diagnostics of electrical machines.